

Electronic Supplementary Information (ESI)

Unraveling and regulating superstructure domain dispersion in lithium-rich layered oxide cathodes for high stability and reversibility

Geunho Choi^{a,b,†}, Ujin Chang^{c,†}, Jeongjae Lee^d, Kwanghee Park^c, Hyuksang Kwon^c, Hyosung Lee^e, Yong-Il Kim^c, Jong Hyeok Seo^c, Yoon-Cheol Park^{a,b}, Inchul Park^{a,b}, Jieun Kim^{a,b}, Seungmi Lee^a, Jinuk Choi^a, Byoungyong Yu^{a,b}, Jun-Hyuk Song^{a,b}, Hosun Shin^c, Seung-Wook Baek^c, Sung Keun Lee^d, Hyeokjun Park^{c,*}, and Keeyoung Jung^{a,*}

^aMaterials Research Division, Research Institute of Industrial Science and Technology (RIST), Pohang, Republic of Korea 37673

^bSecondary Battery Materials Lab, POSCO Holdings N.EX.T Hub, Seoul, Republic of Korea 06194

^cInterdisciplinary Materials Measurement Institute, Korea Research Institute of Standards and Science (KRISS), Daejeon, Republic of Korea 34113

^dSchool of Earth and Environmental Sciences, Seoul National University, Seoul, Republic of Korea 08826

^eDepartment of Measurement Engineering, University of Science and Technology, Daejeon, Republic of Korea 34113

*Corresponding authors at: hjpark@kriis.re.kr (H. Park), keeyoung.jung@rist.re.kr (K. Jung)

† These authors contributed equally to this work.

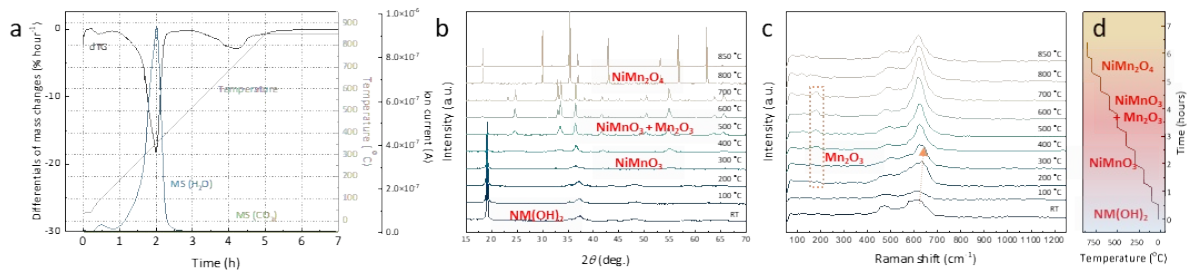


Figure S1. (a) TG-MS analyses results, (b) *in situ* HT-XRD patterns, and (c) *in situ* HT-Raman spectra of $\text{Ni}_{0.33}\text{Mn}_{0.67}\text{O}_2\text{H}_{2-\delta}$ precursor. (d) Graphical illustrations of phase evolution during annealing of $\text{Ni}_{0.33}\text{Mn}_{0.67}\text{O}_2\text{H}_{2-\delta}$ precursor.

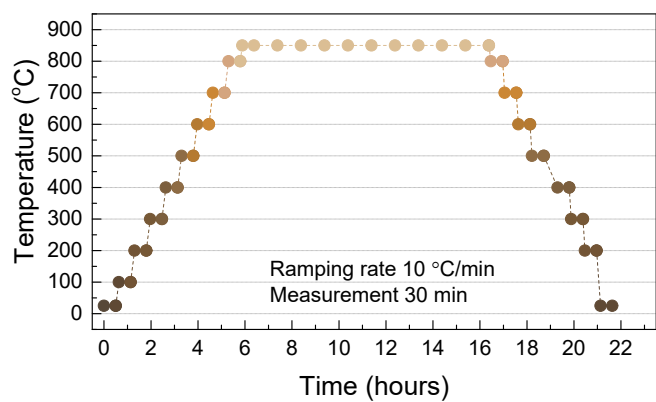


Figure S2. Temperature profile of *in situ* high-temperature measurement experiments.

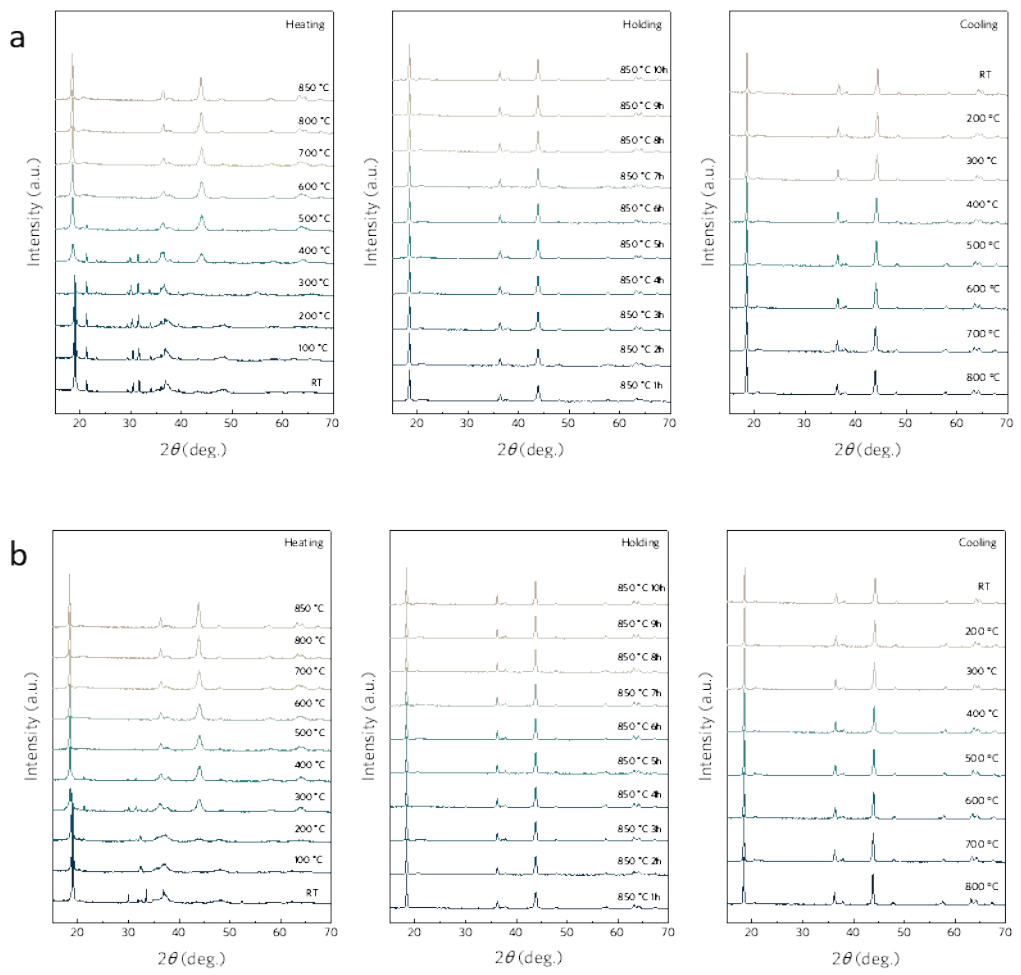


Figure S3. *In situ* HT-XRD patterns for synthetic conditions of heating, holding, and cooling of precursor mixtures with (a) lithium carbonate and (b) lithium hydroxide monohydrate.

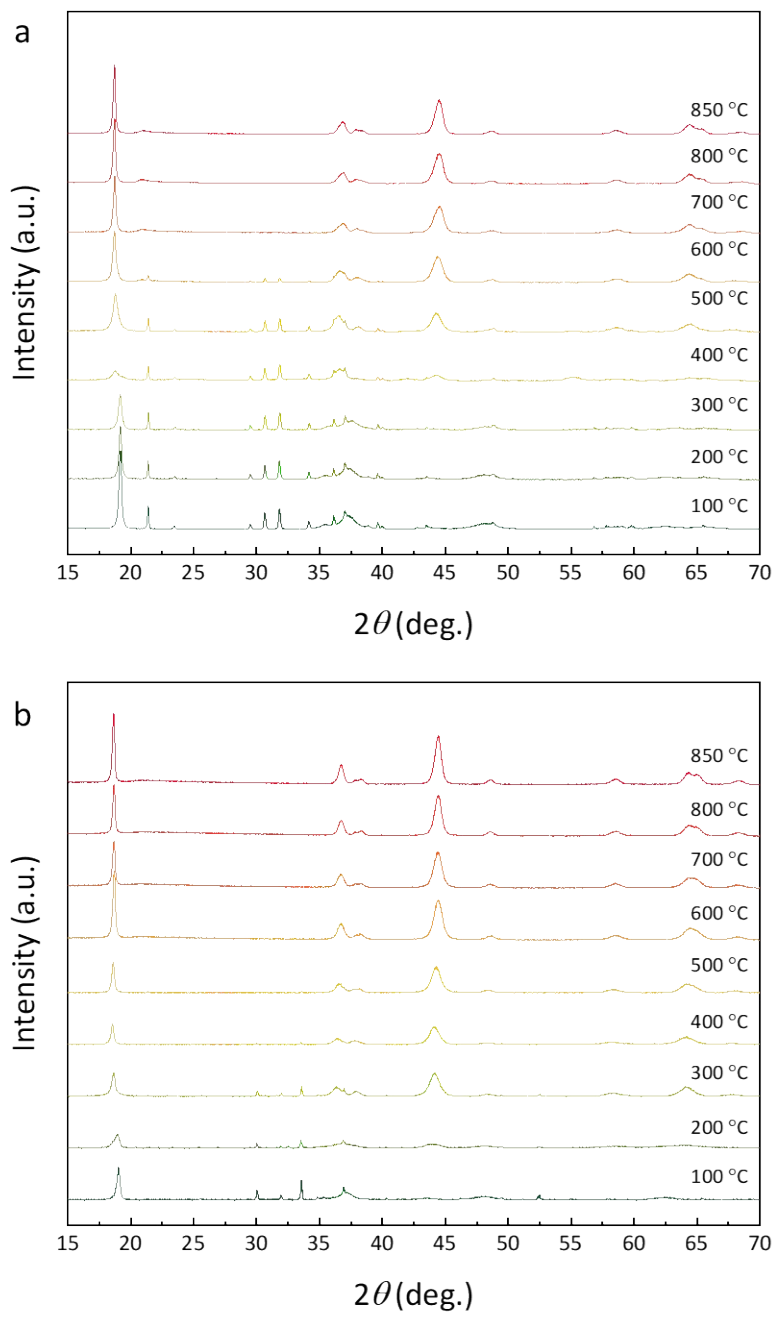


Figure S4. *Ex situ* XRD patterns of precursor mixtures prepared by annealing at given temperature with (a) lithium carbonate and (b) lithium hydroxide monohydrate.

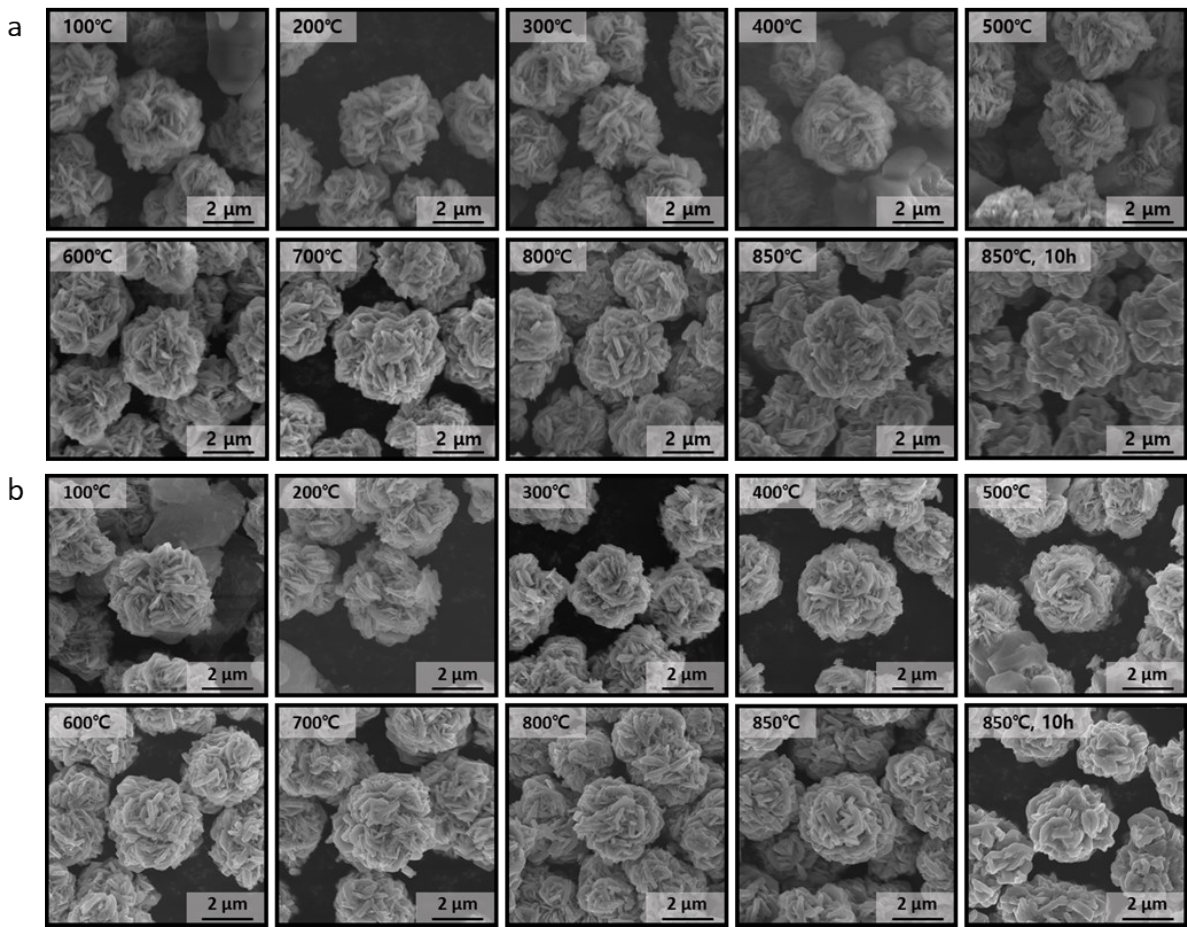


Figure S5. *Ex situ* SEM images of precursor mixtures prepared by annealing at given temperature with (a) lithium carbonate and (b) lithium hydroxide monohydrate.

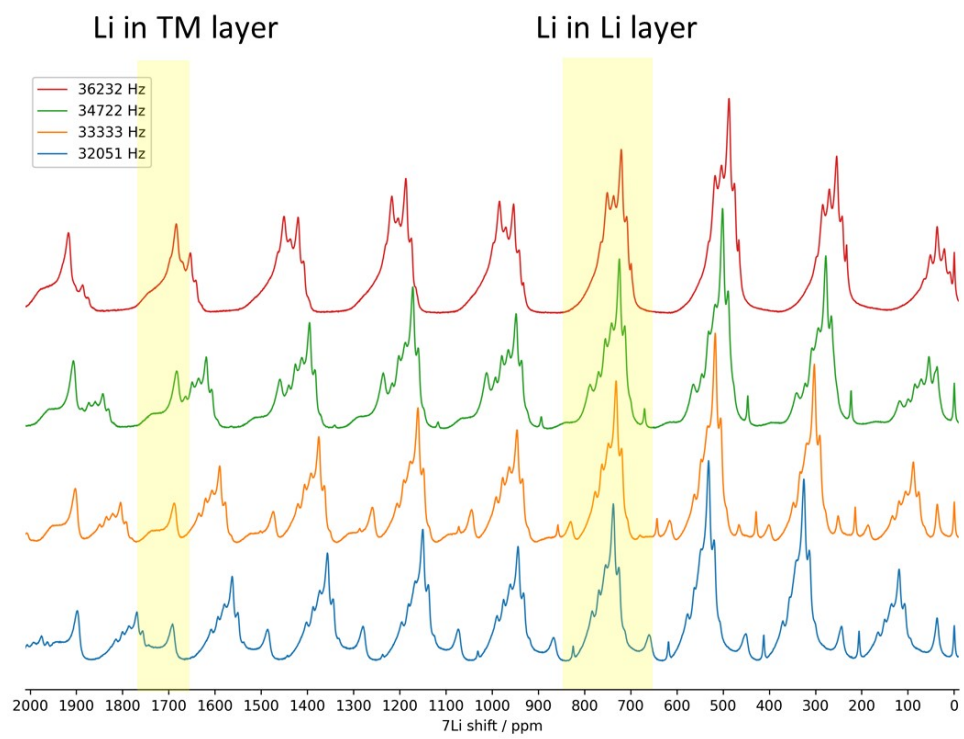


Figure S6. ${}^7\text{Li}$ MAS NMR spectra of LLO with modulation of the frequency. Isotropic chemical shifts were confirmed.

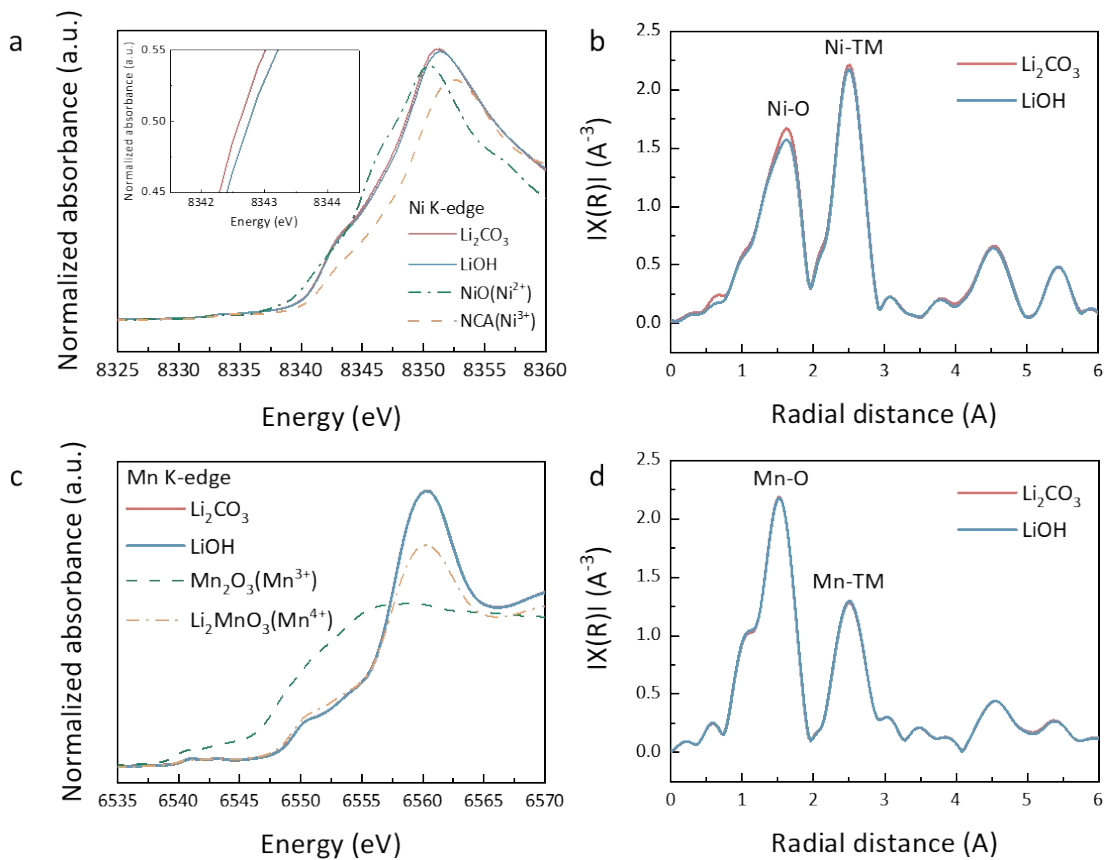


Figure S7. XAS spectra of LLO prepared with lithium carbonate and lithium hydroxide monohydrate. (a) Ni K-edge XANES spectra, (b) Ni K-edge EXAFS spectra, (c) Mn K-edge XANES spectra, (d) Mn K-edge EXAFS spectra. The oxidation state and local structure for Mn are almost identical for the two samples. Subtle differences were observed in the Ni K-edge XAS, where Ni is slightly oxidized in LLO by LiOH with a slight reduction of the Ni–O bond intensity. This might also be relevant to the structural characteristics from the relatively disordered structure of LLO by LiOH than Li_2CO_3 which might include more stacking faults at phase boundaries.

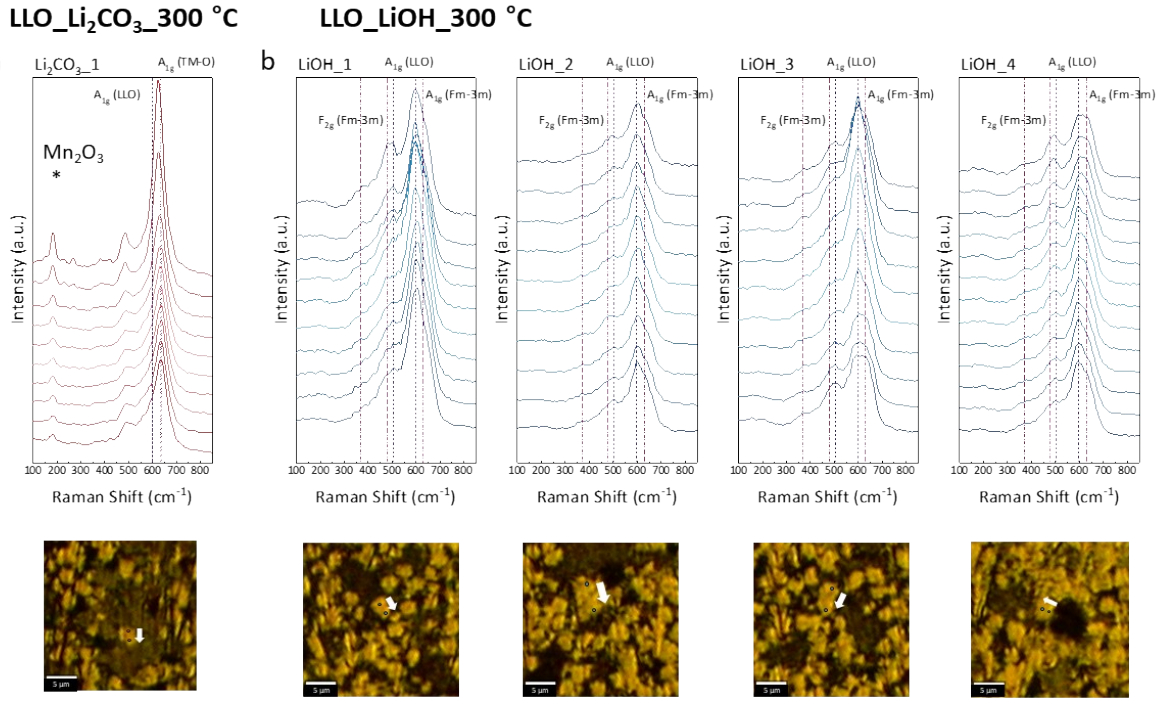


Figure S8. *Ex situ* Raman spectra of multiple particles in cross-section samples of precursor mixture heated at 300°C of (a) lithium carbonate and (b) lithium hydroxide monohydrate.

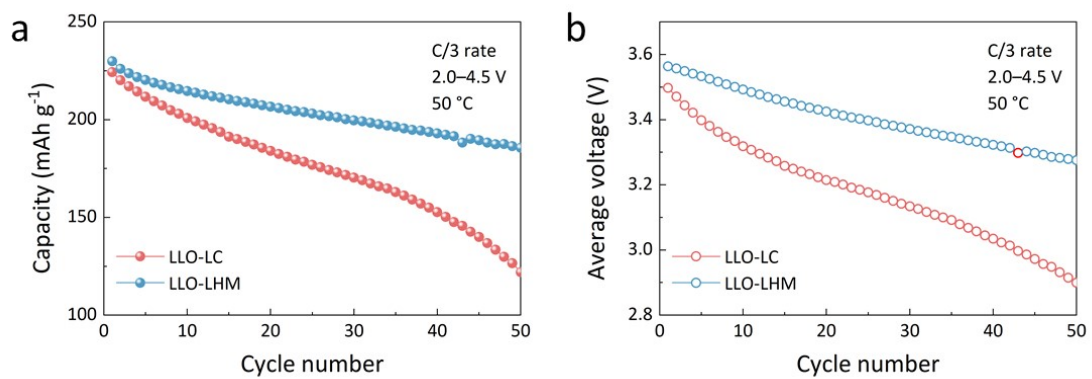


Figure S9. (a) Capacity and (b) average voltage of cells with LLO cathodes during cycling with a cut-off to 4.5 V at high temperature (50 °C).

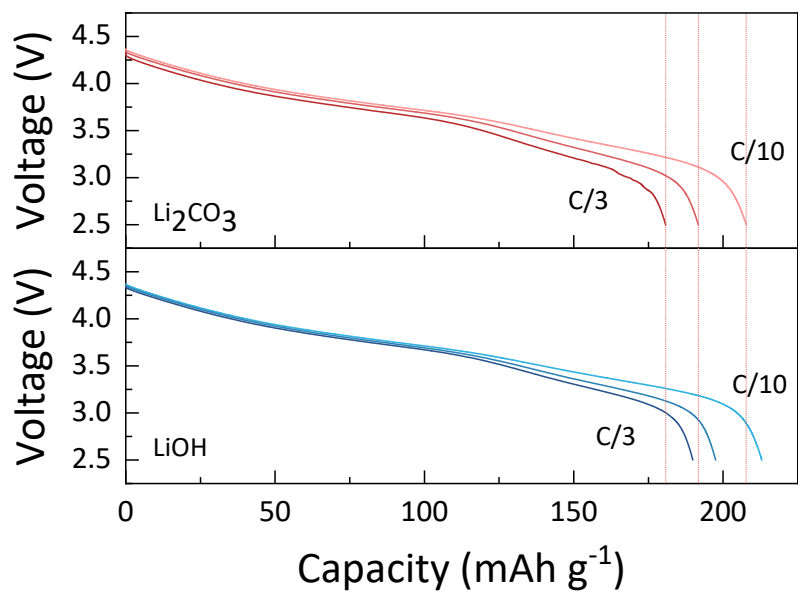


Figure S10. Discharge voltage profiles for LLO cathodes prepared with lithium carbonate and lithium hydroxide monohydrate at different current rates from C/10 to C/3.

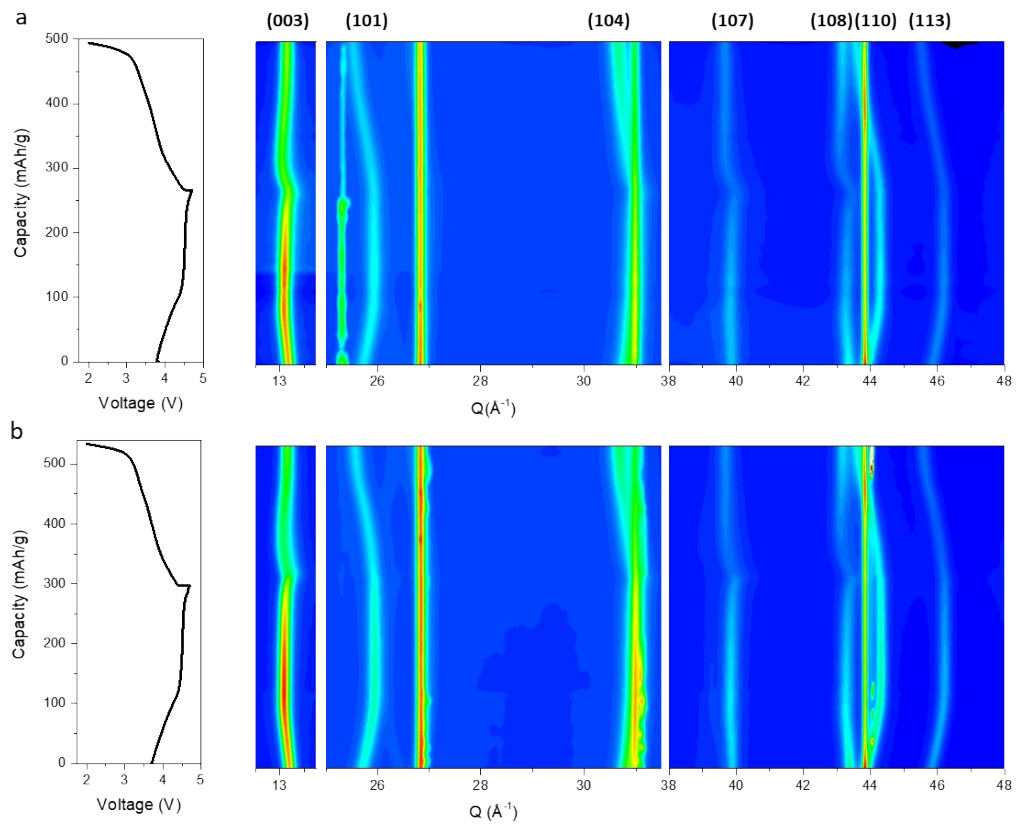


Figure S11. Voltage profiles and full *in situ* synchrotron XRD patterns measured for LLO cathodes prepared with (a) lithium carbonate and (b) lithium hydroxide monohydrate.

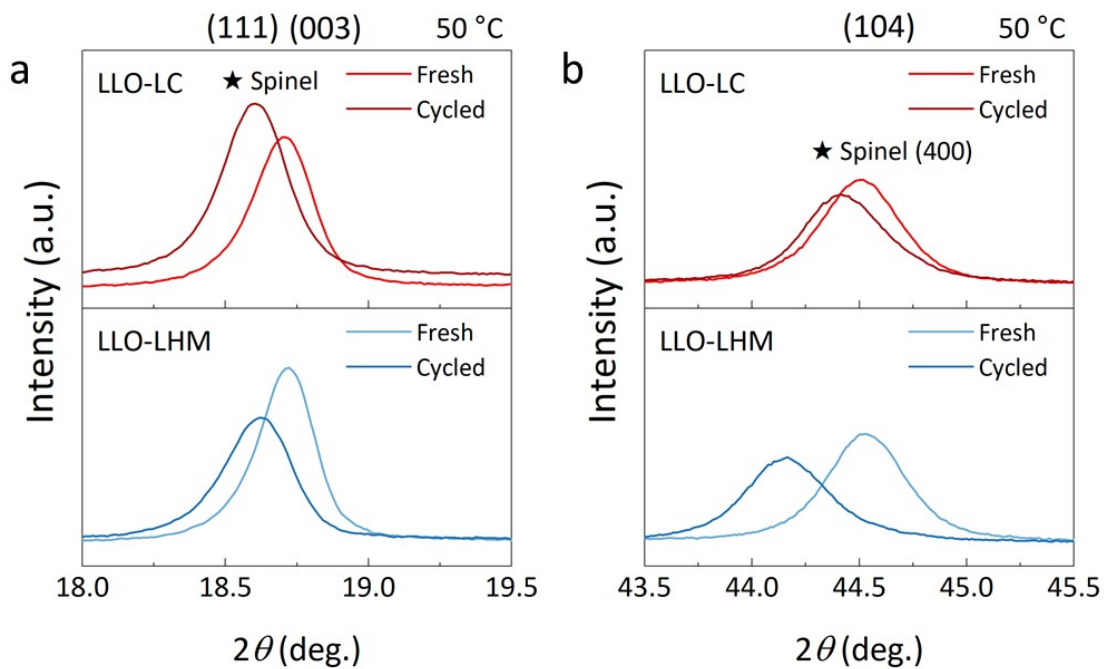


Figure S12. XRD patterns of LLO cathodes before and after cycling at high temperature (50°C).

Table S1. Structural information of LLO-LC based on Rietveld refinement results of X-ray powder diffraction data at 297 K. The symbols, g and B_{eq} , represent the occupation factor and the isotropic thermal parameter, respectively. The numbers in parentheses are the estimated standard deviations of the last significant figure.

$R_{\text{wp}} = 10.92 \%$, $R_{\text{p}} = 8.00 \%$, and GOF (goodness of fit) = 1.65

LiTMO ₂ (TM = Ni, Mn)						
Atom	site	x	y	z	g	$B_{\text{eq}}/\text{\AA}^2$
Li1	3a	0.0	0.0	0.0	0.982(5) ^{a)}	1.1(3)
Ni1	3a	0.0	0.0	0.0	0.018(5)	2.6(2)
Ni2	3b	0.0	0.0	0.5	0.4898(3)	1.1(3)
Mn2	3b	0.0	0.0	0.5	0.5102(3)	1.5(2)
O	6c	0.0	0.0	0.2445(2)	1.0	1.0(1)

Space group: $R\text{-}3\text{ m}$ (No. 166) and $Z = 3$

$a = 2.8667(1)$, $b = 2.8667(1)$ Å and $c = 14.2642(2)$ Å, $\alpha (= \beta) = 90^\circ$, $\beta = 120^\circ$

Li ₂ MnO ₃						
Atom	Site	x	y	z	g	$B_{\text{eq}}/\text{\AA}^2$
Li	2b	0.0	1/2	0.0	1.0	1.5(3)
Li	2c	0.0	0.0	1/2	1.0	1.5(2)
Li	4h	0.0	0.681(1)	1/2	1.0	1.5(3)
Mn	4g	0.0	0.156(2)	0.0	1.0	0.5(2)
O	4i	0.225(9)	0.0	0.196(1)	1.0	1.2(4)
O	8j	0.241(2)	0.322(1)	0.203(6)	1.0	1.3(4)

Space group: $C\text{ 1 2/m 1}$ (No. 12) and $Z = 4$

$a = 4.911(1)$, $b = 8.542(5)$ Å and $c = 5.091(1)$ Å, $\alpha (= \gamma) = 90^\circ$, $\beta = 107.01(13)$

Phase fraction		
LiTMO ₂ (TM = Ni, Mn)		Li ₂ MnO ₃
73.0(1) %		27.0(1) %

a) Constraint on occupancy: $g(\text{Li1}) + g(\text{Ni1}) = 1.0$, $g(\text{Ni2}) + g(\text{Mn2}) = 1.0$

Table S2. Structural information of LLO-LHM based on Rietveld refinement results of X-ray powder diffraction data at 297 K. The symbols, g and B_{eq} , represent the occupation factor and the isotropic thermal parameter, respectively. The numbers in parentheses are the estimated standard deviations of the last significant figure.

$R_{\text{wp}} = 11.95 \%$, $R_{\text{p}} = 8.53 \%$, and GOF (goodness of fit) = 1.73

LiTMO ₂ (TM = Ni, Mn)						
Atom	site	x	y	z	g	$B_{\text{eq}}/\text{\AA}^2$
Li1	3a	0.0	0.0	0.0	0.994(3) ^{a)}	1.5(4)
Ni1	3a	0.0	0.0	0.0	0.006(3)	2.6(3)
Ni2	3b	0.0	0.0	0.5	0.4982(2)	1.3(2)
Mn2	3b	0.0	0.0	0.5	0.5018(2)	1.4(4)
O	6c	0.0	0.0	0.2447(3)	1.0	1.1(1)

Space group: $R\text{-}3\text{ m}$ (No. 166) and $Z = 3$

$a = 2.8663(1)$, $b = 2.8663(1)$ Å and $c = 14.2621(2)$ Å, $\alpha (= \beta) = 90^\circ$, $\beta = 120^\circ$

Li ₂ MnO ₃						
Atom	Site	x	y	z	g	$B_{\text{eq}}/\text{\AA}^2$
Li	2b	0.0	1/2	0.0	1.0	1.6(3)
Li	2c	0.0	0.0	1/2	1.0	1.5(1)
Li	4h	0.0	0.656(1)	1/2	1.0	1.6(2)
Mn	4g	0.0	0.166(4)	0.0	1.0	1.1(2)
O	4i	0.215(6)	0.0	0.216(2)	1.0	1.1(4)
O	8j	0.254(2)	0.314(1)	0.203(2)	1.0	1.4(3)

Space group: $C\text{ 1 2/m 1}$ (No. 12) and $Z = 4$

$a = 4.910(1)$, $b = 8.540(5)$ Å and $c = 5.085(6)$ Å, $\alpha (= \gamma) = 90^\circ$, $\beta = 108.00(12)$

Phase fraction		
LiTMO ₂ (TM = Ni, Mn)		Li ₂ MnO ₃
81.4(1) %		18.6(1) %

a) Constraint on occupancy: $g(\text{Li1}) + g(\text{Ni1}) = 1.0$, $g(\text{Ni2}) + g(\text{Mn2}) = 1.0$